Arch. Mech., **57**, 4, pp. 277–297, Warszawa 2005

Elastic micro-strain energy at the austenite–twinned martensite interface

G. MACIEJEWSKI, S. STUPKIEWICZ, H. PETRYK

Institute of Fundamental Technological Research,
Polish Academy of Sciences
Świętokrzyska 21, 00–049 Warsaw, Poland

A MICROMECHANICAL SCHEME is developed for the analysis of elastic micro-strains induced by local incompatibilities at the austenite-twinned martensite interface. The aim of the paper is to estimate the elastic micro-strain energy which is an important factor in the formation of microstructures during the martensitic transformation. The finite deformation framework is applied, consistent with the crystallographic theory of martensite, and full account is taken for elastic anisotropy of the phases. As an example, the microstructures in the cubic-to-orthorhombic transformation in CuAlNi shape memory alloy are analyzed by the finite element method for the assumed class of zigzag shapes of the austenite-martensite interface at the micro-level. Finally, the effect of the interphase boundary energy on the microstructure of the transition layer is studied.

1. Introduction

ENGINEERING MATERIALS at a suitable scale of observation are usually heterogeneous and thus characterized by some microstructure; often different microstructures can be observed in the same material at different scales of observation. Consequently, the interfaces separating different elements of the microstructure (grains, precipitates, twins, etc.) constitute a common feature of microstructured materials. The related interfacial energies can be of different origin and are recognized to be important factors affecting the properties of these materials as well as the formation and evolution of microstructures. In particular, the characteristic microstructural dimensions can be governed by the relations between different kinds of interfacial and bulk energies. The behaviour of advanced materials can be to much extent determined by the interfacial phenomena. This is, for example, the case for nano-materials in which the role of interfacial energies increases with decreasing grain size. Interfacial phenomena are also essential in materials that undergo phase transformations.

This paper is concerned with martensitic microstructures in shape memory alloys. The unusual effects, such as the shape memory effect and pseudoelasticity, observed in these materials, are associated with martensitic phase transformations which can be induced either by changing temperature or by applied

mechanical loading, see for example OTSUKA and WAYMAN [16] and Bhattacharya [3]. Martensitic transformation is a diffusionless phase transformation between a high temperature, high symmetry parent phase and a low temperature, low symmetry product phase, called austenite and martensite, respectively. Due to the change of symmetry the austenite can transform to several *martensite variants* which are crystallographically equivalent but rotated with respect to each other.

A stress-free interface between austenite and a crystallographically perfect single variant of martensite is usually not possible during progressive transformation due to the lack of kinematic compatibility between these phases at zero stress (as discussed below). For this reason the martensitic transformation is usually accompanied either by twinning (*internally twinned martensites*) or by stacking faults (*internally faulted martensites*).

In the case of internally twinned martensites, studied in this paper, the martensite appears as a fine mixture of two twin-related variants. The classical description of the related microstructure at the austenite-martensite interface, cf. Fig. 1, is provided by the *phenomenological theory of martensitic transformation* of WECHSLER, LIEBERMAN and READ [26], and Bowles and MacKenzie [4], which later has been rigorously reformulated within the nonlinear thermoelasticity theory by BALL and JAMES [1]. The latter theory is called the *crystallographic theory of martensite*. According to this theory, the requirement of displacement continuity is applied at zero stress and implies that the deformation gradients on both sides of the unstressed martensite-martensite interface (twinning plane) and austenite-martensite interface (habit plane) are rank-one connected. Thus, assuming that the elastic strains are equal to zero, the corresponding conditions can be written, cf. BALL and JAMES [1], in the form of the *twinning equation*,

$$\mathbf{Q}\mathbf{U}_I - \mathbf{U}_J = \mathbf{a} \otimes \mathbf{l}, \tag{1.1}$$

and the *habit plane equation*,

$$\hat{\mathbf{Q}}[\lambda \mathbf{Q}\mathbf{U}_I - (1-\lambda)\mathbf{U}_J] - \mathbf{I} = \mathbf{b} \otimes \mathbf{m}. \tag{1.2}$$

Here $\mathbf{U}_I$ and $\mathbf{U}_J$ are the transformation stretch tensors of martensite variants I and J, known from the crystallography of the transformation. The unknowns are the twinning plane and habit plane normal vectors, respectively $\mathbf{l}$ and $\mathbf{m}$, the twinning shear vector $\mathbf{a}$, the shape strain vector $\mathbf{b}$, the twin fraction λ and rotation tensors $\mathbf{Q}$ and $\hat{\mathbf{Q}}$. The solution method for equations (1.1) and (1.2) can be found, for example, in BALL and JAMES [1] and BHATTACHARYA [2]. The microstructures satisfying the twinning equation (1.1) and the habit plane equation (1.2) will be called *compatible*, meaning that they satisfy compatibility conditions (1.1) and (1.2) at zero stress.

The habit plane Eq. (1.2) is a *macroscopic* compatibility condition relating the deformation gradient of austenite, taken as the identity tensor, and the *average* deformation gradient of twinned martensite, i.e. the term in square bracket in Eq. (1.2). Thus, the microstructure predicted by the theory provides macroscopic compatibility at the austenite-martensite interface at zero macroscopic stresses. However, the transformation stretches $\mathbf{U}_I$ and $\mathbf{U}_J$ of the martensite variants, when taken separately, are not compatible with undeformed austenite across *any* interface. This local incompatibility must be accommodated by non-zero local elastic strains (micro-strains) accompanied by related micro-stresses which, in accord with the Saint-Venant rule, can be expected to be effectively concentrated within a relatively thin transition layer, schematically depicted in grey in Fig. 1. It is the corresponding elastic strain energy that is the subject of this work.

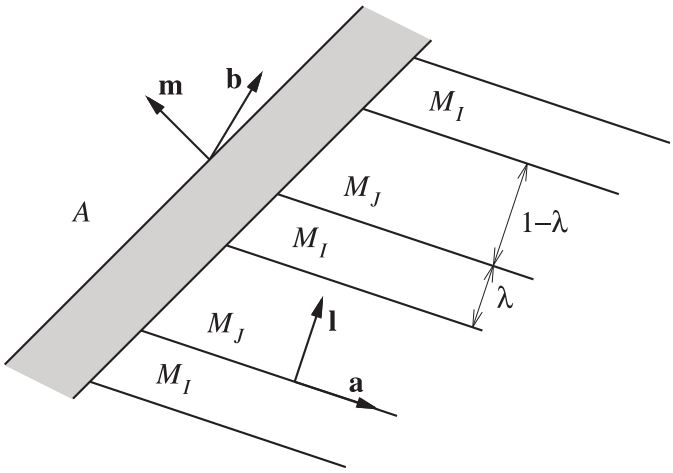

FIG. 1. Microstructure at the austenite–twinned martensite interface (A – austenite, M_I, M_J – martensite variants, in grey – a transition layer).

It is well recognized that the elastic micro-strain energy decreases as the twin spacing decreases, and that the actual dimensions of the microstructures are the result of the interplay of this energy and the interfacial energy of twin boundaries, see for example KHACHATURYAN [10], KOHN and MÜLLER [11], PETRYK *et al.* [17]. The tendency of the material to minimize the total energy may lead to twin branching (i.e. the refinement of twin spacing in the vicinity of the austenite-martensite interface) as well as to the formation of complex microstructures of the transition layer itself. This is studied theoretically and also observed in experiments, cf. BALL and JAMES [1], JAMES *et al.* [9], KOHN and MÜLLER [11], LIU and DUNNE [13].

The elastic micro-strain energy can be computed for an *a priori* assumed microstructure of the transition layer by solving the problem of theory of elasticity with the eigenstrains being constant and given within each phase. For example, SRIDHAR *et al.* [21] presented an analytical solution for a simple microstructure (with the phases occupying rectangular domains) in the case of linear elasticity, the whole system being elastically isotropic and homogeneous. A simple estimate of the elastic micro-strain energy, calibrated using the results of SRIDHAR *et al.* [21], has been provided by ROYTBURD [18].

A more general approach is proposed in this work. A micromechanical analysis performed with the help of the finite element method is carried out to estimate the elastic micro-strain energy at the austenite-twinned martensite interface. The finite deformation setting is used, and the analyzed microstructures are compatible with the predictions of the crystallographic theory. Further, the elastic anisotropy of the phases is fully accounted for and a class of non-planar local austenite-martensite interfaces is considered. Finally, the effect of interfacial energy of interphase austenite-martensite boundaries on the elastic micro-strain energy and on the local interface shape is studied. To illustrate applicability of the proposed approach the case of austenite-martensite interface in the cubic-to-orthorhombic ($\beta_1 \to \gamma_1'$) transformation in a CuAlNi shape memory alloy is examined. A simple zigzag shape of the local austenite-martensite interface is assumed in the numerical example, but more complex microstructures of the transition layer can also be studied using the present approach.

The paper is organized as follows. In Sec. 2 the continuum framework is developed and the variational problem for the representative volume element of a periodic microstructure is formulated. A unit cell suitable for the analysis of the transition layer is defined and some remarks on the finite element implementation are provided. The results of finite element simulations of the microstructures in a CuAlNi single crystal are reported in Sec. 3. Finally, the effect of interfacial energy of interphase boundaries on the elastic micro-strain energy and on the microstructure of the transition layer is studied in Sec. 4.

2. Micromechanical framework

2.1. Continuum formulation and variational problem

Consider a representative volume element (RVE) of a material with a periodic microstructure induced by martensitic phase transformation. The RVE occupies a domain $\mathcal{R}$ of volume V in the reference configuration. The macroscopic (overall) deformation gradient $\bar{\mathbf{F}}$ is given by

$$\bar{\mathbf{F}} = \{\mathbf{F}\}, \qquad \{\cdot\} \equiv \frac{1}{V}\int_{\mathcal{R}} (\cdot)\,\mathrm{d}\mathbf{X}, \tag{2.1}$$

where $\{\cdot\}$ denotes the averaging operation in the reference configuration. The local deformation gradient $\mathbf{F}$,

$$\mathbf{F} = \nabla\boldsymbol{\varphi} = \bar{\mathbf{F}} + \nabla\tilde{\boldsymbol{\varphi}}, \tag{2.2}$$

is defined by the local deformation mapping $\mathbf{x} = \boldsymbol{\varphi}(\mathbf{X})$, such that

$$\boldsymbol{\varphi}(\mathbf{X}) = \bar{\mathbf{F}}\mathbf{X} + \tilde{\boldsymbol{\varphi}}(\mathbf{X}). \tag{2.3}$$

Here $\tilde{\boldsymbol{\varphi}}$ is the displacement fluctuation field such that $\{\tilde{\boldsymbol{\varphi}}\} = 0$.

In the assumed absence of other contributions to the deformation, the deformation gradient $\mathbf{F}$ can be multiplicatively decomposed into its elastic and transformation (i.e. inelastic) parts, $\mathbf{F}^{\mathrm{e}}$ and $\mathbf{F}^{\mathrm{t}}$, respectively, so that

$$\mathbf{F} = \mathbf{F}^{\mathrm{e}}\mathbf{F}^{\mathrm{t}}. \tag{2.4}$$

The inelastic deformation gradient $\mathbf{F}^{\mathrm{t}}$ is related to the shape change of crystalline lattice during martensitic transformation and defines the intermediate stress-free configuration. For austenite, we take $\mathbf{F}^{\mathrm{t}} = \mathbf{I}$, the identity tensor, and for martensite variant I we take $\mathbf{F}^{\mathrm{t}} = \mathbf{F}^{\mathrm{t}}_I$, where $\mathbf{F}^{\mathrm{t}}_I$ is known from the crystallography of transformation and $\mathbf{U}^2_I = \mathbf{F}^T_I\mathbf{F}_I$. For any pair (I, J) of martensite variants, their deformation gradients due to transformation are related by $\mathbf{F}^{\mathrm{t}}_J = \mathbf{Q}_{IJ}\mathbf{F}^{\mathrm{t}}_I\mathbf{Q}^T_{IJ}$, where $\mathbf{Q}_{IJ}$ is a proper orthogonal tensor belonging to the symmetry point group of austenite.

The local constitutive relation is specified by the elastic strain energy function, per unit volume in the reference configuration, assumed here in the form

$$W(\mathbf{F}) = \frac{1}{2}(\det\mathbf{F}^{\mathrm{t}})\,\mathbf{E}^{\mathrm{e}}\cdot\mathbf{L}\mathbf{E}^{\mathrm{e}}, \tag{2.5}$$

where $\mathbf{E}^{\mathrm{e}} = \dfrac{1}{2}(\mathbf{F}^{\mathrm{e}T}\mathbf{F}^{\mathrm{e}} - \mathbf{I})$ is the elastic Green strain tensor and $\mathbf{L}$ is the elastic moduli tensor, both referring to the intermediate stress-free configuration. Note that juxtaposition of a second-order tensor and either another one or a vector means simple contraction, while a fourth-order tensor followed by a second-order one denotes here double contraction. Double contraction of two second-order tensors is indicated by a central dot.

Equation (2.5) is a simple generalization of anisotropic elasticity at infinitesimal strain to the case of finite strains of sufficiently small magnitude. In fact, in the problem examined here the elastic strains are so small that the choice of an elastic strain measure is not essential, and the use of W as a convex quadratic function in $\mathbf{E}^{\mathrm{e}}$ (but *not* in $\mathbf{F}$) is justified. At the same time the effects of finite rotations and finite $\mathbf{F}^{\mathrm{t}}$ are treated correctly.

The specific form of the elastic strain energy function (2.5) of austenite is

$$W_{\mathrm{A}}(\mathbf{F}) = \frac{1}{2}\,\mathbf{E}^{\mathrm{e}} \cdot \mathbf{L}_{\mathrm{A}}\mathbf{E}^{\mathrm{e}}, \qquad \mathbf{F}^{\mathrm{e}} = \mathbf{F}, \tag{2.6}$$

and that of martensite variant I is

$$W_I(\mathbf{F}) = \frac{1}{2}(\det \mathbf{F}^{\mathrm{t}}_I)\,\mathbf{E}^{\mathrm{e}} \cdot \mathbf{L}_I\mathbf{E}^{\mathrm{e}}, \qquad \mathbf{F}^{\mathrm{e}} = \mathbf{F}(\mathbf{F}^{\mathrm{t}}_I)^{-1}. \tag{2.7}$$

Note that the elastic moduli tensors of martensite variants I and J are symmetry-related, i.e. $(L_J)_{ijkl} = (Q_{IJ})_{ip}(Q_{IJ})_{jq}(Q_{IJ})_{kr}(Q_{IJ})_{ls}(L_J)_{pqrs}$. A material point within the RVE, except on the interfaces, may thus take one of $N+1$ possible material states (the austenite and N variants of martensite). Once the microstructure (i.e. spatial arrangement of different phases within the RVE) is specified, the spatial distribution of the material properties, $\mathbf{F}^{\mathrm{t}}(\mathbf{X})$ and $\mathbf{L}(\mathbf{X})$, is given, as $\mathbf{F}^{\mathrm{t}}$ and $\mathbf{L}$ are known for each phase.

The local nominal stress $\mathbf{S}$ and, for a self-equilibrated field $\mathbf{S}$ (Hill [7]), the macroscopic one $\bar{\mathbf{S}}$ are given by

$$\mathbf{S} = \frac{\partial W}{\partial \mathbf{F}}, \qquad \bar{\mathbf{S}} = \{\mathbf{S}\}, \tag{2.8}$$

while the macroscopic density of elastic strain energy is a functional defined for any piecewise differentiable field $\tilde{\boldsymbol{\varphi}}$ as

$$\bar{W} = \bar{W}(\bar{\mathbf{F}}, \tilde{\boldsymbol{\varphi}}) = \{W\}. \tag{2.9}$$

We assume periodicity of the microstructure, which implies that the boundary $\partial\mathcal{R}$ can be divided into two parts $\partial\mathcal{R}^+$ and $\partial\mathcal{R}^-$ such that $\partial\mathcal{R} = \partial\mathcal{R}^+ \cup \partial\mathcal{R}^-$, $\partial\mathcal{R}^+ \cap \partial\mathcal{R}^- = 0$ and

$$\tilde{\boldsymbol{\varphi}}^+ = \tilde{\boldsymbol{\varphi}}^-\,, \qquad \mathbf{t}^+ = -\mathbf{t}^-\,, \tag{2.10}$$

where $\tilde{\boldsymbol{\varphi}}^\pm$ and $\mathbf{t}^\pm$ are, respectively, displacement fluctuations and nominal tractions at the corresponding points on $\partial\mathcal{R}^+$ and $\partial\mathcal{R}^-$.

Let us introduce the total potential energy $\mathit{\Pi}$ as a sum of the elastic strain energy and the potential energy of the applied loading, namely

$$\Pi(\bar{\mathbf{F}}, \tilde{\boldsymbol{\varphi}}) = \bar{W}(\bar{\mathbf{F}}, \tilde{\boldsymbol{\varphi}}) - \mathbf{S}^* \cdot \bar{\mathbf{F}}\,, \tag{2.11}$$

where $\mathbf{S}^*$ is a *prescribed* macroscopic nominal stress. At mechanical equilibrium $\mathit{\Pi}$ is stationary with respect to $\bar{\mathbf{F}}$ and $\tilde{\boldsymbol{\varphi}}$, however, $\tilde{\boldsymbol{\varphi}}$ must additionally satisfy the periodicity constraint, $\tilde{\boldsymbol{\varphi}}^+ = \tilde{\boldsymbol{\varphi}}^-$. Let us thus define the Lagrangian $\mathcal{L}$,

$$\mathcal{L}(\bar{\mathbf{F}}, \tilde{\boldsymbol{\varphi}}, \boldsymbol{\mu}) = \Pi(\bar{\mathbf{F}}, \tilde{\boldsymbol{\varphi}}) - \frac{1}{V}\int\limits_{\partial\mathcal{R}^+} \boldsymbol{\mu} \cdot (\tilde{\boldsymbol{\varphi}}^+ - \tilde{\boldsymbol{\varphi}}^-)\,\mathrm{d}S\,, \tag{2.12}$$

where $\boldsymbol{\mu}$, the Lagrange multiplier field defined on $\partial\mathcal{R}^+$, is introduced to enforce the periodicity constraint; the value of $\tilde{\boldsymbol{\varphi}}^-$ is obviously taken at a point on $\partial\mathcal{R}^-$ corresponding to that on $\partial\mathcal{R}^+$.

This leads in a standard way to the variational equality obtained by taking the Gateaux derivative of $\mathcal{L}$ equal to zero, namely

$$\begin{aligned}(2.13)\qquad \mathrm{D}\mathcal{L}(\bar{\mathbf{F}},\tilde{\boldsymbol{\varphi}},\boldsymbol{\mu};\delta\bar{\mathbf{F}},\delta\tilde{\boldsymbol{\varphi}},\delta\boldsymbol{\mu}) &= (\bar{\mathbf{S}}(\bar{\mathbf{F}},\tilde{\boldsymbol{\varphi}})-\mathbf{S}^*)\cdot\delta\bar{\mathbf{F}} \\ &+\frac{1}{V}\left[\int_{\mathcal{R}}\mathbf{S}(\bar{\mathbf{F}},\tilde{\boldsymbol{\varphi}})\cdot\nabla\delta\tilde{\boldsymbol{\varphi}}\,\mathrm{d}V-\int_{\partial\mathcal{R}^+}\boldsymbol{\mu}\cdot(\delta\tilde{\boldsymbol{\varphi}}^+-\delta\tilde{\boldsymbol{\varphi}}^-)\,\mathrm{d}S\right. \\ &\left.-\int_{\partial\mathcal{R}^+}\delta\boldsymbol{\mu}\cdot(\tilde{\boldsymbol{\varphi}}^+-\tilde{\boldsymbol{\varphi}}^-)\,\mathrm{d}S\right]=0\quad\forall\,\delta\bar{\mathbf{F}},\ \forall\,\delta\tilde{\boldsymbol{\varphi}},\ \forall\,\delta\boldsymbol{\mu}.\end{aligned}$$

We note that for $\bar{\mathbf{F}}$, $\tilde{\boldsymbol{\varphi}}$ and $\boldsymbol{\mu}$ satisfying the equilibrium and periodicity conditions all the terms on the right-hand side of (2.13) vanish. Note also that the Lagrange multipliers $\boldsymbol{\mu}$ have the interpretation of nominal tractions acting on the boundary $\partial\mathcal{R}$, so that $\mathbf{t}^+=\boldsymbol{\mu}$, $\mathbf{t}^-=-\boldsymbol{\mu}$.

Concluding, for given $\mathbf{S}^*$, the solution of the variational problem (2.13) provides the macroscopic deformation gradient $\bar{\mathbf{F}}$, the displacement fluctuation field $\tilde{\boldsymbol{\varphi}}$ and Lagrange multipliers $\boldsymbol{\mu}$ such that the RVE is in equilibrium and the macroscopic stress is equal to the prescribed stress $\mathbf{S}^*$, i.e. $\bar{\mathbf{S}}=\mathbf{S}^*$. In particular, $\mathbf{S}^*$ can be set equal to zero.

2.2. Unit cell for the analysis of the transition layer

As already mentioned in the Introduction, the aim of this paper is to investigate the elastic micro-strains in the transition layer at the austenite-twinned martensite interface. Accordingly, the discussion below is restricted to the case of internally twinned martensites.

The basic microstructure element of stress-induced martensites is a twinned martensitic plate, i.e. a plate-like inclusion within the austenite matrix. In the simplest case the transformation proceeds by the formation of a family of parallel plates. The microstructure is then a rank-two laminate as the plates are themselves laminates of twin-related martensite variants. Such microstructures appear when the transformation is induced by a macroscopic stress, so that the layers of austenite and martensite are stressed. The mismatch of elastic properties (naturally expected to exist due to different anisotropy of parent and product phases) leads to development of additional residual stresses in the layers (STUPKIEWICZ and PETRYK [23]). Moreover, if detwinning (i.e. mobility of

twin boundaries) is allowed during transformation the residual stresses may be even higher due to the variation of twin fraction and the related incompatibility of the effective transformation strain of the martensitic plate. This is related to the reduced shear resistance of twinned martensite associated with twinning deformation (ROYTBURD and SLUTSKER [20], STUPKIEWICZ and PETRYK [24]). Note also that the microstructural parameters (habit plane orientation, twin fraction, etc.) of martensitic plates formed under stress may deviate from those predicted by the crystallographic theory in the stress-free conditions (ROYTURD and PANKOVA [19], OLIVER *et al.* [14], Stupkiewicz [22]).

The situation is quite different when the martensitic transformation is induced by stress-free cooling from austenitic state. The microstructures are geometrically more complex as, in addition to differently oriented plates, microstructures such as wedges and self-accommodating groups may appear (BHATTACHARYA [2, 3]). However, in all these cases the austenite and martensite can coexist through the basic austenite-twinned martensite microstructure of Fig. 1 conforming to the crystallographic theory (1.1)–(1.2). Also, in agreement with the assumptions of the crystallographic theory the elastic strains and the stresses are expected to (practically) vanish sufficiently far from the interface (i.e. outside the transition layer).

Consider now a periodic laminated microstructure formed by parallel plates of twinned martensite in the austenite matrix. The microstructure is defined by the following microstructural parameters: $\mathbf{l}$, $\mathbf{m}$, λ, h and H; where h and H are, respectively, the twin spacing and the plate spacing as shown in Fig. 2 a. Parameters $\mathbf{l}$, $\mathbf{m}$ and λ satisfy the twinning and habit plane Eqs. (1.1)–(1.2), so that the microstructure is *compatible*. In macroscopically stress-free conditions the transition layer in this laminate is fully representative for the austenite-twinned martensite interfaces of other stress-free microstructures with the periodic arrangement of twins, provided that the spacing H of neighbouring austenite-martensite interfaces is sufficiently large relative to twin spacing h. The stresses are expected to decay exponentially with the distance from the interface (cf. SRIDHAR *et al.* [21]) so that the requirement of sufficiently large H/h (which amounts to the requirement that the interaction of neighbouring austenite-martenisite interfaces is negligible) can easily be satisfied in practice. Also, assuming that the elastic energy decays similarly with the distance from the interface towards austenite and towards martensite, the uniform spacing of austenite-martensite interfaces (which corresponds to the volume fraction of martensite $\eta = 0.5$) is the most natural choice. Note that for the present purpose the actual values of parameters H/h and η can be taken arbitrarily as long as the solution in the transition layer is practically not sensitive to their variation. Once the microstructure is defined, the solution of the variational problem (2.13) for a unit cell such as that shown in Fig. 2 b provides the distrib-

ution of the elastic energy in the transition layer which can further be integrated to yield the macroscopic interfacial energy associated with the elastic micro-strains.

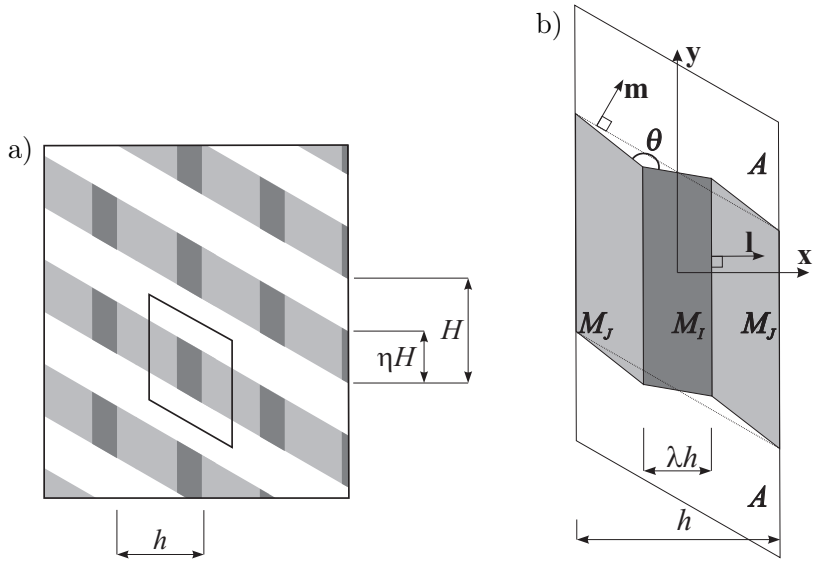

FIG. 2. Schematic view of the analyzed laminated microstructure.

When the macroscopic stress is not equal to zero, as in the case of stress-induced transformation, or when the microstructure is not compatible, so that residual stresses develop everywhere, the situation is more complex. The deformation of the laminated microstructure consists of uniform stress and strain fields with superimposed non-uniform fields in the transition layer. Formally, the elastic micro-strain energy can be defined as the difference between the total energy of the actual microstructured material and the energy of uniform states weighted by respective volume fractions of austenite and martensite variants, viz.

$$\bar{W}^* = \bar{W} - (1-\eta)W_{\mathrm{A}}(\mathbf{F}_{\mathrm{A}}) - \eta[\lambda W_I(\mathbf{F}_I) + (1-\lambda)W_J(\mathbf{F}_J)], \tag{2.14}$$

where $\mathbf{F}_{\mathrm{A}}$, $\mathbf{F}_I$ and $\mathbf{F}_J$ are the uniform parts of the deformation gradients in austenite and martensite variants I and J, respectively. These deformation gradients may be determined by solving the micro-macro transition relationships for laminates (generalizing the small strain analysis of STUPKIEWICZ and PETRYK [23]) or, alternatively, they may be approximated by the respective deformation gradients far from the austenite-martensite interface obtained by the numerical solution of the variational problem (2.13).

It should be noted that even for a fixed microstructure the elastic micro-strain energy (2.14) depends on the external stress $\mathbf{S}^*$, because of the adopted finite deformation kinematics and nonlinear constitutive relationship (2.5)–$(2.8)_1$. This

dependence is, however, expected to be negligible in view of the elastic strains being relatively small. Note that within the linear elasticity framework, the elastic micro-strain energy is constant for fixed microstructure of the transition layer and independent of the macroscopic stress and volume fraction of martensite (as long as the distance between the neighbouring interfaces is sufficiently large for their interaction to be negligible). In the following, only the macroscopic stress-free situation is considered, and the dependence of $\bar{W}^*$ on the external stress is not pursued any more.

The real shape of the austenite-martensite interface at the micro level can be rather complex, see for example LIU and DUNNE [13], HÝTCH *et al.* [8]. In this work, as a first approximation, we consider a zigzag-shaped interface as shown in Fig. 2 b) with the orientation of the macroscopic (i.e. average) austenite-martensite interface determined by the habit plane normal $\mathbf{m}$. The zigzag shape is fully characterized by the wedge angle θ indicated in Fig. 2 b. The planar interface corresponds thus to $\theta = 180$ [deg].

The adopted microstructure is in fact two-dimensional as it does not change in the direction perpendicular to $\mathbf{l}$ and $\mathbf{m}$. A two-dimensional *generalized plane strain* analysis can thus be carried out within the plane specified by these two vectors. The global Cartesian coordinate system is adopted such that the x- and y-axes lie in that plane, x-axis being aligned with $\mathbf{l}$. Thus, the displacement fluctuation field $\tilde{\boldsymbol{\varphi}}$ does not depend on z-coordinate, so that

$$\tilde{\boldsymbol{\varphi}} = \tilde{\boldsymbol{\varphi}}(x, y). \tag{2.15}$$

However, note that $\tilde{\boldsymbol{\varphi}}(x, y)$ is a field of three-dimensional vectors, so that locally a fully three-dimensional stress state occurs.

Once the unit cell with periodic boundary conditions is defined, e.g. such as that shown in Fig. 2 b), the elastic energy associated with the elastic micro-strains in the transition layer can be computed from formula (2.14) using the scheme of Sec. 2.1 with the unit cell as RVE at zero macroscopic stress, i.e. by putting $\mathbf{S}^* = \mathbf{0}$, cf. Eq. (2.13). In particular, if the microstructural parameters are determined from the compatibility equations (1.1) and (1.2), i.e. for the compatible microstructure, then $\bar{W}^*$ at $\mathbf{S}^* = \mathbf{0}$ reduces simply to $\bar{W}$. When $\bar{W}^*$ is computed, the related interfacial energy γ_{e} can be determined from

$$\gamma_{\mathrm{e}} = \frac{V}{A}\,\bar{W}^*, \tag{2.16}$$

where A is the nominal area of the *macroscopic* austenite-martensite interfaces (habit planes) contained within the periodic cell. We note that the interfacial energy γ_{e} depends on the size of the periodic cell. More specifically, it follows from dimensional analysis that γ_{e} is proportional to the twin spacing h. The proportionality factor Γ_{e},

$$\Gamma_{\mathrm{e}} = \frac{\gamma_{\mathrm{e}}}{h}, \tag{2.17}$$

can thus be introduced which is a characteristic (size-independent) quantity of the considered microstructure. Parameter Γ_{e} depends on the microstructure of the transition layer and, for the assumed class of zigzag shapes, on angle θ.

2.3. Finite element implementation

Let us introduce a finite element discretization of displacement fluctuations $\tilde{\boldsymbol{\varphi}}$ within the domain $\mathcal{R}$ and of Lagrange multipliers $\boldsymbol{\mu}$ on the boundary $\partial\mathcal{R}^+$,

$$\tilde{\boldsymbol{\varphi}}^h = \sum_i N_i \tilde{\boldsymbol{\varphi}}_i\,, \qquad \boldsymbol{\mu}^h = \sum_i N_i^{\mu} \boldsymbol{\mu}_i\,, \tag{2.18}$$

where $\tilde{\boldsymbol{\varphi}}_i$ and $\boldsymbol{\mu}_i$ are the nodal quantities and N_i and N_i^{μ} are the corresponding shape functions.

The discretized problem for the unknown nodal quantities $\tilde{\boldsymbol{\varphi}}_i$ and $\boldsymbol{\mu}_i$ follows from the condition of a stationary point of $\mathcal{L}^h = \mathcal{L}(\bar{\mathbf{F}}, \tilde{\boldsymbol{\varphi}}^h, \boldsymbol{\mu}^h)$, cf. Eqns. (2.12) and (2.13), namely

$$\frac{\partial \mathcal{L}^h}{\partial \bar{\mathbf{F}}} = \mathbf{S}^*\,, \qquad \frac{\partial \mathcal{L}^h}{\partial \tilde{\boldsymbol{\varphi}}_i} = \mathbf{0}\,, \qquad \frac{\partial \mathcal{L}^h}{\partial \boldsymbol{\mu}_i} = \mathbf{0}\,. \tag{2.19}$$

Equations (2.19) constitute a system of nonlinear algebraic equations for the unknown $\{\bar{\mathbf{F}}, \tilde{\boldsymbol{\varphi}}_i, \boldsymbol{\mu}_i\}$. Note that, in addition to nodal displacement fluctuations $\tilde{\boldsymbol{\varphi}}_i$ and Lagrange multipliers $\boldsymbol{\mu}_i$, the macroscopic deformation gradient $\bar{\mathbf{F}}$ is an unknown of the problem.

The system of nonlinear equations (2.19) can be solved using the iterative Newton scheme. This part is very standard thus the details are omitted here.

Two types of finite elements are developed: solid finite elements modelling the material behaviour according to (2.2)–(2.5) and $(2.18)_1$ and additional elements used to enforce the periodicity conditions with the Lagrange multipliers interpolated on the boundary $\partial\mathcal{R}^+$ according to $(2.18)_2$. For the reason of computational efficiency, in the latter case, the method of augmented Lagrangians is used rather than the classical Lagrange multiplier technique. Thus the augmented Lagrangian functional is introduced in the form

$$\mathcal{L}_{\mathrm{aug}}(\bar{\mathbf{F}}, \tilde{\boldsymbol{\varphi}}, \boldsymbol{\mu}) = \mathcal{L}(\bar{\mathbf{F}}, \tilde{\boldsymbol{\varphi}}, \boldsymbol{\mu}) + \frac{1}{V} \int\limits_{\partial\mathcal{R}^+} \frac{\rho}{2} (\tilde{\boldsymbol{\varphi}}^+ - \tilde{\boldsymbol{\varphi}}^-) \cdot (\tilde{\boldsymbol{\varphi}}^+ - \tilde{\boldsymbol{\varphi}}^-)\, \mathrm{d}S, \tag{2.20}$$

where $\rho > 0$ is a regularization parameter. The computational scheme follows that outlined above, Eqs. (2.18)–(2.19), with $\mathcal{L}$ replaced by $\mathcal{L}_{\mathrm{aug}}$.

The generalized plane strain solid elements interpolate the three-dimensional displacement fluctuations $\tilde{\boldsymbol{\varphi}}$ over a two-dimensional domain in the (x, y)-plane. Here isoparametric 8-node serendipity elements are used with 3×3 Gauss integration scheme. The Lagrange multiplier term defined along $\partial\mathcal{R}^+$ in (2.12) is integrated nodally using a 3-point Lobatto scheme.

Note that the z-axis is a two-fold symmetry axis of the periodic cell, cf. Fig. 2 b. Thus the model of the whole periodic cell with periodicity constraints enforced along its opposite edges, can equivalently be replaced by one half of the cell, say the upper half, with periodicity constraints enforced for the left and right edge of the cell and with anti-periodicity constraints enforced along the top and bottom edges. Clearly, the latter case is computationally more efficient as the same accuracy can be achieved for the size of the problem reduced by, approximately, the factor of two.

The FE implementation has been performed within the *Computational Templates* environment using a symbolic code generation system *AceGen* [12]. The FE procedures are written in a high-level computer language of *Mathematica* [27] taking advantage of the additional functionality of *AceGen* (i.e. automatic differentiation technique, automatic code generation, simultaneous optimization of expressions and theorem proving by stochastic evaluation of the expressions) and of *Computational Templates* environment (templates for automatic generation of FE procedures based on the symbolic description of the problem).

3. Finite element computations

3.1. Material properties

In this section the elastic micro-strain energy is analyzed for the cubic-to-orthorhombic $\beta_1 \rightarrow \gamma_1'$ transformation in a CuAlNi alloy. In this transformation six martensite variants exist with a total of 96 different austenite-twinned martensite microstructures, cf. HANE and SHIELD [6]. However, all the microstructures can be divided into four groups of 24 microstructures in a group, such that the microstructures belonging to the same group are crystallographically equivalent, i.e. they are related by the symmetry point group of the cubic parent phase. Thus four microstructures, one from each group, sufficiently characterize all the possible microstructures.

The parameters of four crystallographically distinct microstructures that follow from the crystallographic theory, Eqs. (1.1)–(1.2), corresponding to the twin pair ($I = 1$, $J = 3$) are provided in Table 1 (vector components refer to the cubic basis of austenite). The respective transformation stretch tensor components of martensite variants in the cubic basis of austenite are

$$U_1 = \begin{pmatrix} (\alpha+\gamma)/2 & 0 & (\alpha-\gamma)/2 \\ 0 & \beta & 0 \\ (\alpha-\gamma)/2 & 0 & (\alpha+\gamma)/2 \end{pmatrix},$$

(3.1)

$$U_3 = \begin{pmatrix} (\alpha+\gamma)/2 & (\alpha-\gamma)/2 & 0 \\ (\alpha-\gamma)/2 & (\alpha+\gamma)/2 & 0 \\ 0 & 0 & \beta \end{pmatrix},$$

where the stretch parameters $\alpha = 1.0619$, $\beta = 0.9178$ and $\gamma = 1.0230$ are computed from the lattice parameters provided by OTSUKA and SHIMIZU [15].

Table 1. Microstructures in the $\beta_1 \to \gamma_1'$ transformation in CuAlNi ($I = 1$, $J = 3$).

Type I twins

	Microstructure M1	Microstructure M2
λ	0.2902	0.2902
l	$(0., 0.7071, -0.7071)$	$(0., 0.7071, -0.7071)$
a	$(0.05153, 0.16374, 0.18688)$	$(0.05153, 0.16374, 0.18688)$
m	$(0.6350, 0.7486, 0.1908)$	$(-0.7151, 0.6497, -0.2579)$
b	$(0.06564, -0.06574, 0.02385)$	$(-0.05760, -0.07476, -0.01710)$

Type II twins

	Microstructure M3	Microstructure M4
λ	0.3008	0.3008
l	$(-0.2282, -0.6884, -0.6884)$	$(-0.2282, -0.6884, -0.6884)$
a	$(0.00358, -0.16909, 0.19205)$	$(0.00358, -0.16909, 0.19205)$
m	$(-0.6345, -0.7276, -0.2607)$	$(0.7304, -0.6679, 0.1430)$
b	$(-0.06530, 0.06539, -0.01219)$	$(0.05595, 0.07070, 0.02367)$

The elastic constants of single-crystalline austenite and martensite of CuAlNi, measured by SUEZAWA and SUMINO [25] and YASUNAGA *et al.* [28], are given in Table 2.

The microstructural parameters **l**, **m** and λ provided in Table 1 define the geometry of the unit cell used in the computations and, in particular, the global coordinate system in which the analysis is carried out. The components of the inelastic deformation gradient tensors, $\mathbf{F}_1^{\mathrm{t}} = \mathbf{U}_1$ and $\mathbf{F}_3^{\mathrm{t}} = \mathbf{U}_3$, and the components of elastic moduli tensors in this coordinate system are obtained by applying proper rotations from the local coordinate system associated with the cubic basis of austenite to the global one.

Table 2. Elastic constants of CuAlNi single crystals.

Cubic β_1 phase[a]

c_{11}	c_{12}	c_{44} [GPa]
142	126	96

[a)] SUEZAWA and SUMINO (1976)

Orthorhombic γ_1' phase[b]

c_{11}	c_{22}	c_{33}	c_{44}	c_{55}	c_{66}	c_{12}	c_{13}	c_{23} [GPa]
189	141	205	54.9	19.7	62.6	124	45.5	115

[b)] YASUNAGA *et al.* (1983)

3.2. Results

The geometry of the unit cell is defined by the microstructural parameters of Table 1, and by the geometrical parameters such as the wedge angle θ determining the zigzag shape of the interface, the volume fraction of martensite η ($\eta = 0.5$ is used), and the ratio of plate spacing to twin spacing, H/h. The value of $H/h = 40$ has been adopted for the computations (further increase of H/h by the factor of two results in the increase of the energy by less than 0.01 per cent).

A structured mesh of 56×64 8-node elements with the total of about 34000 degrees of freedom has been used to discretize one half of the unit cell. The mesh has been significantly refined in the vicinity of the austenite-martensite interface and in particular in the vicinity of the triple junctions (i.e. points of intersection of twinning planes and austenite-martensite boundaries), as the solutions at these points are expected to be singular. For example, a logarithmic singularity is predicted in the case of linear isotropic elasticity, cf. e.g. EVANS *et al.* [5]. No attempt has been made to include the singularities into the present finite element model. However, it has been verified that the total elastic strain energy does not change appreciably with further mesh refinement.

The results of the finite element computations are summarized in Fig. 3 where the computed values of parameter $\Gamma_{\rm e}$ as a function of angle θ are shown for the four microstructures of Table 1. The dashed line at $\theta = 180$ [deg] indicates the case of a planar interface. We note that the effect of the wedge angle θ on the micro-strain energy is significant. For example, in the case of microstructure M2, the minimum value of $\Gamma_{\rm e}$ (at $\theta \approx 55$ [deg]) is less than half of that corresponding to the planar interface, see Table 3 where selected values of parameter $\Gamma_{\rm e}$ are provided for comparison. The shapes of the minimum energy interfaces are shown in Fig. 4 for the four microstructures.

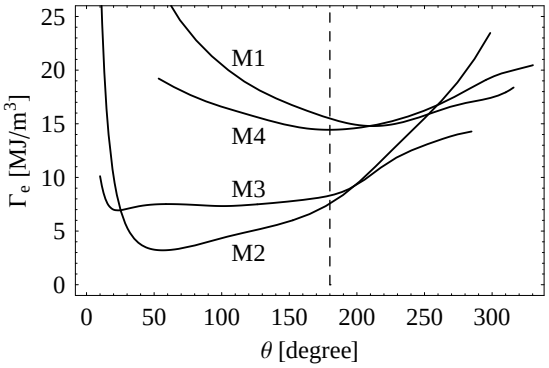

FIG. 3. Elastic micro-strain energy parameter Γ_e as a function of the wedge angle θ of a zigzag-shaped austenite-twinned martensite interface.

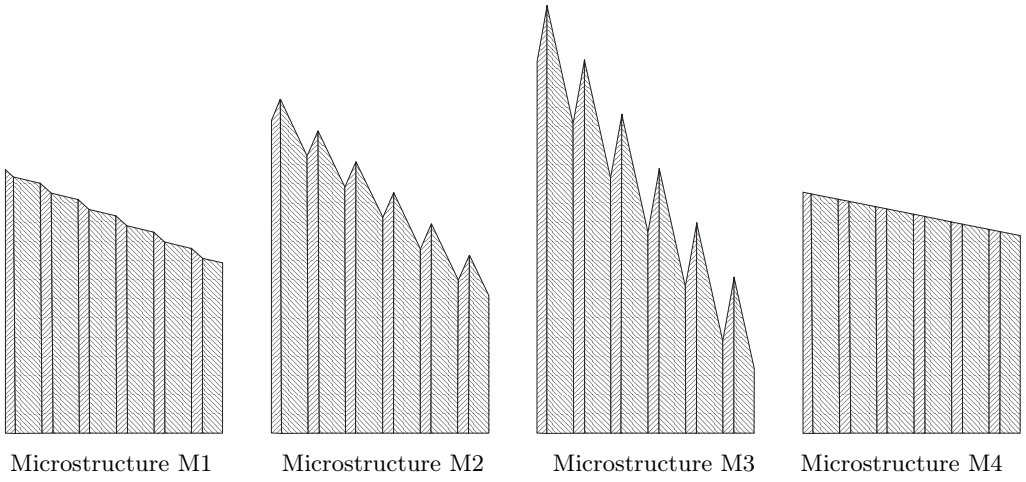

FIG. 4. Austenite-twinned martensite interface shapes corresponding to the minimum values of elastic micro-strain energy parameter Γ_e, cf. Fig. 3.

As expected, the elastic strains and the elastic strain energy are concentrated in the vicinity of the austenite-martensite interface. This is illustrated in Fig. 5 where the distributions of the elastic energy density W and of a sample elastic Green strain component E^e_{yy} are shown within the transition layer of the minimum energy interface in microstructure M2. Note that the maximum values of W and E^e_{yy} indicated in Fig. 5 are mesh-dependent in view of expected singularity at the triple junctions.

In order to check the effect of elastic properties of the phases on the elastic micro-strain energy, the transition layer with a planar interface has additionally been analyzed assuming that martensite has the elastic properties of austen-

ite (elastically homogeneous case), cf. Table 3. It can be seen that the elastic heterogeneity effect is in most cases smaller than the effect of the interface shape.

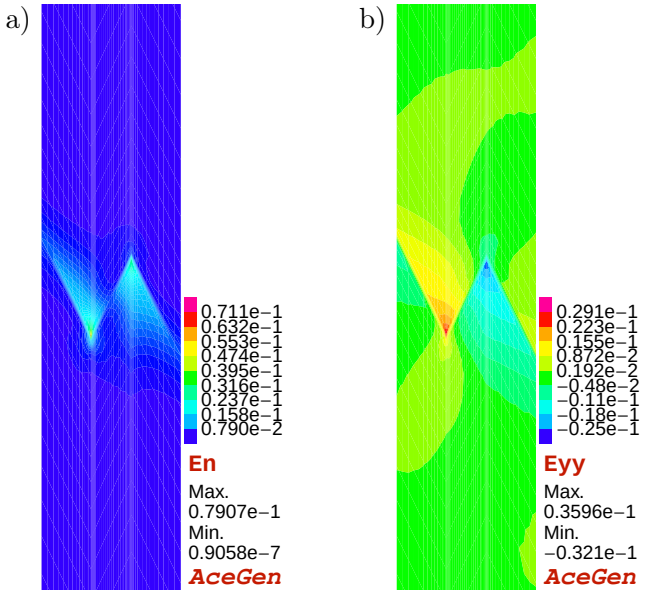

FIG. 5. Distribution of a) elastic energy density W and b) elastic Green strain tensor E^{e}_{yy} in the vicinity of austenite-martensite interface in microstructure M2.

Table 3. Selected values of parameter Γ_{e}.

Γ_{e} [MJ/m^3]	M1	M2	M3	M4
minimum	14.8	3.2	6.9	14.4
planar interface	15.5	7.6	8.3	14.4
planar interface, elastically homogeneous	16.1	7.8	8.3	15.7

4. The effect of interphase boundary energy

It is frequently assumed that the microstructures formed during the transformation minimize the total free energy. The elastic micro-strain energy studied in the previous section naturally contributes to the total energy of a material undergoing phase transformation.

But clearly it is not the only kind of energy related to formation of the microstructure. For example, the twin boundary energy is an important parameter

affecting the characteristic dimensions of real microstructures, such as twin spacing h, cf. e.g. KOHN and MÜLLER [11], PETRYK *et al.* [17]. However, as long as twin branching is not considered, the twin boundary energy has no direct effect on the microstructure pattern of the transition layer.

Below, another parameter, namely the energy of austenite-martensite interphase boundaries and its effect on the microstructure of the transition layer, is studied on the basis of numerical results of the previous section. We take now into account also the interfacial energy γ_{aI} of the boundaries between austenite and single martensite variants at the micro-level.

Consider thus the interfacial energy density per unit nominal area of the habit plane,

$$\gamma_i = \Gamma_e h + \psi \gamma_{aI} \,, \tag{4.1}$$

which is the sum of the elastic micro-strain energy $\gamma_e = \Gamma_e h$ and of the energy of interphase boundaries $\psi\gamma_{aI}$, where $\psi = \psi(\theta) \geq 1$ is the ratio of the real area of the zigzag-shaped interface to the nominal area of austenite-twinned martensite interface. Parameter ψ is a purely geometrical factor dependent here only on θ for fixed $\mathbf{l}$, $\mathbf{m}$ and λ. Note that the interphase boundary energy γ_{aI} can in general depend on the relative orientation of crystalline lattices and on the orientation of the boundary. Here, due to the lack of respective experimental data, this energy is assumed to be identical for both variants of martensite, i.e. for both orientations of local austenite-martensite interfaces, $\gamma_{aI} = \gamma_{aJ}$.

Let us introduce the parameter Γ_i,

$$\Gamma_i = \frac{\gamma_i}{h} = \Gamma_e + \psi \frac{\gamma_{aI}}{h}, \tag{4.2}$$

which depends on γ_{aI} and h only through their ratio γ_{aI}/h. The dependence of Γ_i on angle θ of the zigzag shaped interface and on ratio γ_{aI}/h is shown in Fig. 6 for microstructure M2. The dotted line in Fig. 6 connects the points of minimum Γ_i. As expected, for increasing γ_{aI}/h the angle θ corresponding to the minimum interfacial energy tends to $\theta = 180$ [deg]. This can also be seen in Fig. 7 where the variation of the wedge angle $\theta^{\min}$ corresponding to the minimum of Γ_i is plotted as a function of γ_{aI}/h. The jump visible in Fig. 7 for microstructure M3 is related to the jump from one local minimum to another, cf. the corresponding shape of the graph in Fig. 3.

As it is illustrated in Fig. 8, the relative importance of the two components of the interfacial energy depends on the ratio γ_{aI}/h. In the limit $\gamma_{aI}/h \to \infty$, the energy of interphase boundaries dominates and thus the planar interface minimizes the interfacial energy.

As the final result of this section, the minimum interfacial energy parameter $\Gamma_i^{\min}$ as a function of γ_{aI}/h is shown in Fig. 9 for all the four microstructures. The

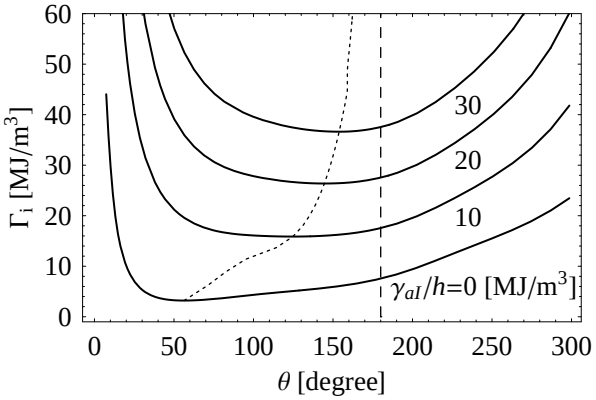

FIG. 6. Interfacial energy parameter Γ_i of microstructure M2 as a function of wedge angle θ for different values of the ratio $\gamma_{\mathrm{a}I}/h$.

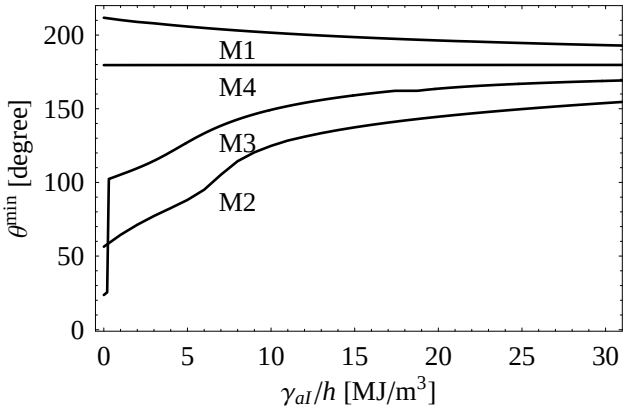

FIG. 7. Wedge angle $\theta^{\min}$ corresponding to the minimum of interfacial energy parameter Γ_i as a function of $\gamma_{\mathrm{a}I}/h$.

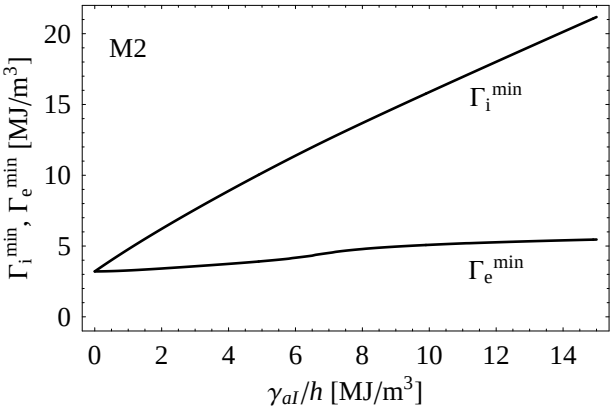

FIG. 8. Minimum interfacial energy parameter $\Gamma_\mathrm{i}^{\min}$ and its part due to elastic micro-strains, Γ_e, as a function of $\gamma_{\mathrm{a}I}/h$ (microstructure M2).

dependence is nearly linear except at low values of $\gamma_{\mathrm{a}I}/h$ where the influence of the elastic-micro strain energy is dominant. It is seen that the interfacial energy of microstructure M2 is lowest in the whole range of parameters $\gamma_{\mathrm{a}I}/h$. This could suggest that microstructure M2 is energetically preferable to microstructures M1, M3 and M4. Note that all four microstructures provide similar macroscopic transformation strains. However, when h is small, the differences between the values of surface densities γ_{i} of different microstructures are relatively small, and other factors may affect the choice of microstructure.

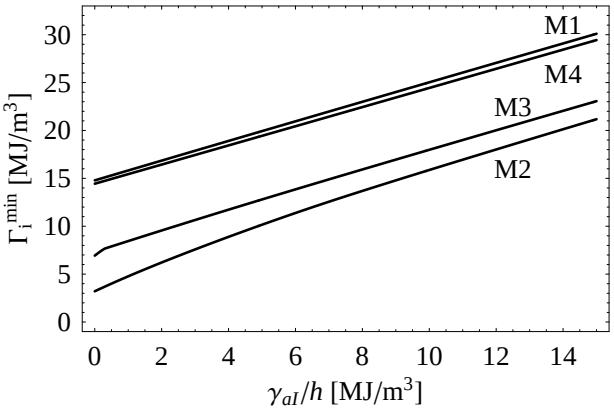

FIG. 9. Minimum interfacial energy parameter $\Gamma_{\mathrm{i}}^{\min}$ as a function of $\gamma_{\mathrm{a}I}/h$ for all analyzed microstructures.

5. Concluding remarks

A method to estimate the elastic micro-strain energy of the transition layer at the austenite-twinned martensite interface has been proposed in the paper. The micromechanical scheme is based on the variational principle for the unit cell of a periodic rank-two laminate and employs the finite deformation framework so that the microstructures predicted by the crystallographic theory of martensite can be consistently analyzed.

As an application, the estimation of the elastic micro-strain energy is provided for the microstructures in the cubic-to-orthorhombic ($\beta_1 \rightarrow \gamma_1'$) transformation in CuAlNi alloy using the available experimental data. A simple class of one-parameter zigzag shapes of the interface at the micro-level is considered. Other shapes of the interface can also be analyzed within the present approach, however, in case of multi-parameter descriptions of the interface shape, optimization techniques must be applied to find the minimum energy shape. Clearly, this is much simpler in the present case of only one shape parameter.

It has been shown that the effect of the interface shape is significant, and that the deviation from planar shape can significantly reduce the elastic micro-strain energy. However, in this context, the energy of austenite-martensite interphase boundaries is also an important parameter affecting the microstructure of the transition layer.

Acknowledgment

This work has been supported by the State Committee for Scientific Research (KBN) in Poland through Grant No. 4 T07A 032 26.

References

1. J.M. Ball and R.D. James, *Fine phase mixtures as minimizers of energy*, Arch. Rat. Mech. An., **100**, 13–50, 1987.
2. K. Bhattacharya, *Wedge-like microstructure in martensites*, Acta Metall. Mater., **39**, 2431–2444, 1991.
3. K. Bhattacharya, *Microstructure of martensite: why it forms and how it gives rise to the shape-memory effect*, Oxford University Press, Oxford 2003.
4. J.S. Bowles and J.K. MacKenzie, *The crystallography of martensitic transformations I and II*, Acta Metall., **2**, 129–137 and 138–147, 1954.
5. A.G. Evans, N. Burlingame, M. Drory, and W.M. Kriven, *Martensitic transformations in zirconia — particle size effects and toughening.*, Acta Metall., **29**, 447–456, 1981.
6. K.F. Hane and T.W. Shield, *Microstructure in a copper-aluminium-nickel shape-memory-alloy*, Proc. R. Soc. Lond. A, **455**, 3901–3915, 1999.
7. R. Hill, *On constitutive macro-variables for heterogeneous solids at finite strain*, Proc. R. Soc. Lond. A, **326**, 131–147, 1972.
8. M.J. Hÿtch, Ph. Vermaut, J. Malarria, and R. Portier, *Study of atomic displacement fields in shape memory alloys by high-resolution electron microscopy*, Mater. Sci. Eng., A273–275, 266–270, 1999.
9. R.D. James, R.V. Kohn, and T.W. Shield, *Modeling of branched needle microstructures at the edge of a martensite laminate*, J. Physique IV, **C8**, 253–259, 1995.
10. A.G. Khachaturyan, *Theory of Structural Transformations in Solids*, John Wiley and Sons, New York 1983.
11. R.V. Kohn and S. Müller *Branching of twins near an austenite–twinned-martensite interface*, Phil. Mag. A., **66**, 5, 697–715, 1992.
12. J. Korelc, *Multi-language and multi-environment generation of nonlinear finite element codes*, Engineering with Computers, **18**, 312–327, 2002.
13. D.Z. Liu and D. Dunne, *Atomic force microscope study of the interface of twinned martensite in copper-aluminium-nickel*, Scripta Mater., **48**, 12, 611–1616, 2003.

14. E.C. OLIVER, N. KOBAYASHI, T. MORI, M.R. DAYMOND, and P.J. WITHERS, *Mechanical energy criterion for stress-induced martensitic transformation*, Scripta Mater., **49**, 1013–1019, 2003.

15. K. OTSUKA and K. SHIMIZU, *Morphology and crystallography of thermoelastic Cu–Al–Ni martensite analyzed by the phenomenological theory*, Trans. Jap. Inst. Metals, **15**, 103–108, 1974.

16. K. OTSUKA and C.M. WAYMAN [Eds.], *Shape memory materials*, Cambridge University Press, 1998.

17. H. PETRYK, S. STUPKIEWICZ, and G. MACIEJEWSKI *Modelling of austenite/martensite laminates with interfacial energy effect*, [in:] Proc. IUTAM Symp. on Size Effects on Material and Structural Behaviour at Micron- and Nanometer-Scales. Hong Kong 2004. (in press).

18. A.L. ROYTBURD, *Thermodynamics of polydomain heterostructures, II Effect of microstresses*, J. Appl. Phys., **83**, 1, 239–245, 1998.

19. A.L. ROYTBURD and M.N. PANKOVA, *The influence of external stresses on the orientation of the habit plane and substructure of stress-induced martensite plates in iron-based alloys*, Fiz. Met. Metalloved., **59**, 4, 769–779, 1985. English translation: Phys. Met. Metall., **59**, 131–140, 1985.

20. A.L. ROYTBURD and J. SLUTSKER, *Deformatin of adaptive materials. Part III: Deformation of crystals with polytwin product phases*, J. Mech. Phys. Solids, **49**, 1795–1822, 2001.

21. N. SRIDHAR, J.M. RICKMAN, and D.J. SROLOVITZ, *Twinning in thin films – I. Elastic analysis. Acta Mater.*, **44**, 10, 4085–4096, 1996.

22. S. STUPKIEWICZ, *The effect of stacking fault energy on the formation of stress-induced internally faulted martensite plates*, Eur. J. Mech. A/Solids, **23**, 1, 107–126, 2004.

23. S. STUPKIEWICZ and H. PETRYK, *Modelling of laminated micro-structures in stress-induced martensitic transformation*, J. Mech. Phys. Solids, **50**, 2303–2331, 2002.

24. S. STUPKIEWICZ and H. PETRYK, *Micromechanical modelling of stress-induced martensitic transformation and detwinning in shape memory alloys*, Journal de Physique IV, **115**, 141–149, 2004.

25. M. SUEZAWA and K. SUMINO, *Behaviour of elastic constants in Cu-Al-Ni alloy in the close vicinity of M_s-point*, Scripta Metall., **10**, 789–792, 1976.

26. M.S. WECHSLER, D.S. LIEBERMAN, and T.A. READ, *On the theory of the formation of martensite*, Trans. AIME J. Metals, **197**, 1503–1515, 1953.

27. S. WOLFRAM, *The Mathematica Book*, 4th ed. Wolfram Media/Cambridge University Press, 1999.

28. M. YASUNAGA, Y. FUNATSU, S. KOJIMA, K. OTSUKA, and T. SUZUKI, *Measurement of elastic constants*, Scripta Metall., **17**, 1091–1094, 1983.

Received October 22, 2004.